

## **Electrochemical Performance of Network Nanocomposite of Spherical Graphite with Various Carbon Conductors**

*X.L. Li\**, *K. Du*, *H. Wang*, *H.F. Song*, *H.D. Liu*, *H.Y. Li*, *Y.X. Zhang*, *J.M. Huang*

College of Materials Science and Engineering, Chongqing University, Chongqing, 400030, P. R. China

\*E-mail: [lixinlu@cqu.edu.cn](mailto:lixinlu@cqu.edu.cn)

*Received:* 4 June 2011 / *Accepted:* 5 September 2011 / *Published:* 1 October 2011

---

A comparative investigation was carried out on three kind of carbonaceous conducting additives in different dimensions, such as carbon black, multiwalled carbon nanotubes and graphene nanosheets, combining with spherical natural graphite as an anode material for lithium ion batteries. Microstructure of the carbon conductors and the corresponding conductive network of electrodes were investigated by XRD, nitrogen adsorption, TEM, and SEM. The anodic performance was tested by cyclic voltammetry and galvanostatic charge-discharge experiments. The results prove that graphene nanosheets are the most effective to improve reversible capacity and cycle stability. The research indicates that graphene nanosheets exhibit the potential application for high-power lithium ion batteries.

---

**Keywords:** Graphite, Carbon conductors, Graphene nanosheets, Lithium ion batteries

### **1. INTRODUCTION**

Lithium ion batteries are playing an increasingly important role in the market of energy storage and conversion devices due to their high energy density and good cycle stability [1, 2]. In the field of lithium ion batteries, much attention has been paid to electrode active materials and conductive additives. According to previous literatures, a certain amount of conductor is usually added to the electrode active particles to enhance the electronic conductivity [3, 4]. At the same time, the microstructure and distribution of conductors can markedly influence electrolyte diffusion [5].

Recently, carbon materials, such as carbon black (CB) and multiwalled carbon nanotubes (MWCNTs) have been widely introduced as conductive additives owing to their electric conductivity and chemical inertness. Jang et al. reported that carbon additives play an important role in electrochemical reaction activity [6, 7]. Li et al. found that the addition of MWCNTs in the electrode preparation would improve the electrochemical capacity [8, 9]. In addition, graphene nanosheets

(GNs), which possess excellent electronic and thermal conductivity, are considered as an ideal candidate for the conductive additives [10].

Different carbon additives vary in crystallinity, morphology and particle size. And the distribution of carbonaceous conductive additives makes a difference in the electron conductivity of the electrode materials. More importantly, the conducting network, combined by electrode active materials and carbon conductors, influence the electrochemical performance a lot. However, previous literatures never reported on the network nanocomposite of andoe active materials with carbon conductors in different dimension. Here will come to systematically compare the different network of spherical graphite mixed with carbonaceous conductive additives, such as zero-dimensional CB, one-dimensional MWCNTs and two-dimensional GNs. The work will focus on the network and the electrochemical performance of the anode composite.

## 2. EXPERIMENTAL

### 2.1. Materials and characterization

Spherical graphite (C: 99.9 wt%,  $D_{50}=10.3\ \mu\text{m}$ ) was provided from Guanqi Company (Henan Province, China). The MWCNTs were purchased from Shenzhen Nanotech Port Co., Ltd (Shenzhen, China) and used as received. Natural flake graphite ( $D_{50}=400\ \mu\text{m}$ ) was offered by Qingdao Taineng Graphite Co., Ltd (Shandong Province, China). GNs were prepared in three steps: firstly, the natural flake graphite was oxidized to graphite oxide via a modified Hummers' method [11], and then rapidly exfoliated at high temperatures under nitrogen atmosphere to obtain the expanded graphite (EG). Finally, the EG was dispersed in ethanol and exfoliated into GNs under a 250 W ultrasonic agitation for 4 hours.

X-ray diffraction (XRD) patterns were obtained from DMAX-2500PC using  $\text{Cu}/\text{K}\alpha$  radiation ( $\lambda=1.5406\ \text{\AA}$ ). Brunauer-Emmett-Teller (BET) specific surface area and pore size distribution was measured by nitrogen absorption using automatic specific surface area measuring equipment (ASAP 2020 M). The morphologies and structures of conductive additives were observed by scanning electron microscope (FEI Nova 400 Nano SEM) and high-resolution transmission electron microscope (HRTEM, LIBRA 200FE).

### 2.2. Battery assembly and electrochemical test

The working anode was prepared by mixing graphite, polyvinylidene fluoride binder and conductive additives (CB or MWCNTs or GNs) in the weight ratio 90:5:5 in N-methyl-2-pyrrolidone solvent. Herein, the graphite mixed with CB, MWCNTs and GNs are labeled as G-CB, G-MWCNTs, and G-GNs, respectively. The charge-discharge characteristics were examined in CR2430 coin cells, assembled in an argon-filled glove box. These cells were composed of a lithium foil as the corresponding electrode, 1 M  $\text{LiPF}_6$  in the volume ratio 1:1 ethyl carbon (EC)/diethyl carbonate (DEC) as the electrolyte, microporous polyethylene separator (Celgard 2500) and the prepared anode.

The cells were galvanostatically charge-discharged in the voltage range from 0.0 to 2.0 V versus Li/Li<sup>+</sup> at 0.1 C rate using NBBAITE Battery Test System. Cyclic voltammetry (CV) was carried out at 0.05 mV/s scanning rate in 0.0-2.0 V versus Li/Li<sup>+</sup> potential range and electrochemical impedance spectroscopy (EIS) was performed from 1 Hz to 100 kHz frequency range using Solartron (1287+1260 8w).

### 3. RESULTS AND DISCUSSION

The XRD patterns of different carbon conductive additives are shown in Fig. 1.

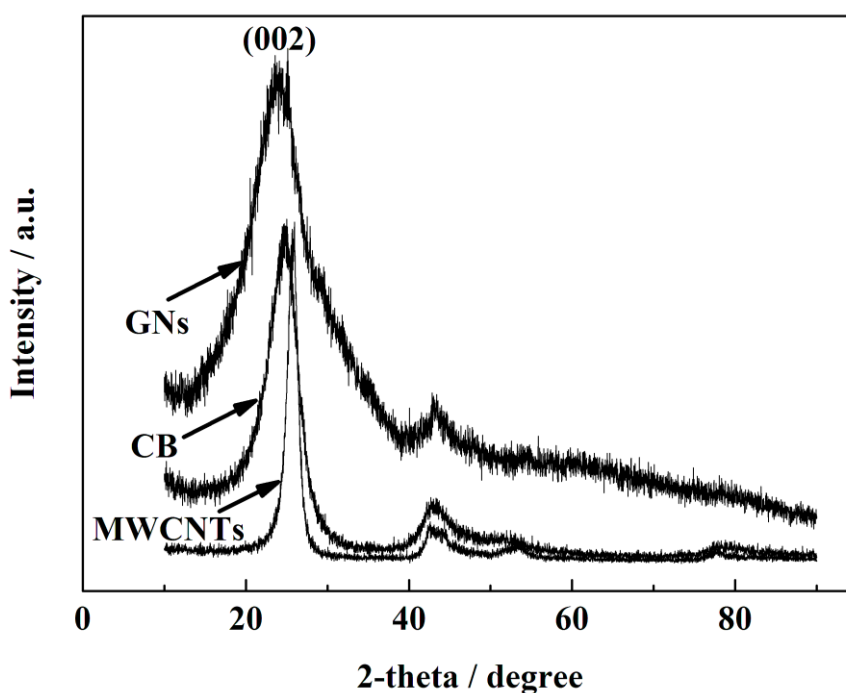


**Figure 1.** XRD patterns of CB, MWCNTs and GNs.

**Table 1.** The structural analysis of the three kind of carbonaceous conductive additives (CB, MWCNTs and GNs).

Structural Characteristics	CB	MWCNTs	GNs
(BET) Specific surface area(m <sup>2</sup> g <sup>-1</sup> )	64.4	109.9	575.3
Total pore volume(cm <sup>3</sup> g <sup>-1</sup> )	0.18	0.42	2.08
Average pore diameter(nm)	10.9	14.0	12.2
The interlayer spacing d(0 0 2)(nm)	0.353	0.344	0.356

The broadened (0 0 2) peak of CB and GNs corresponds to unorganized carbon structures. Researchers have realized that amorphous carbons showed higher specific capacity than ordered graphitic carbons [12]. Based on the calculation of Bragg equation, the interlayer spacing  $d(002)$  in Table 1 is calculated to be 0.353 nm, 0.344 nm, and 0.356 nm for CB, MWCNTs, and GNs, respectively, while the interlayer spacing  $d(002)$  of the natural flake graphite is 0.337 nm. The higher interlayer spacing of GNs is induced by extensive oxidation and rapid thermal exfoliation.

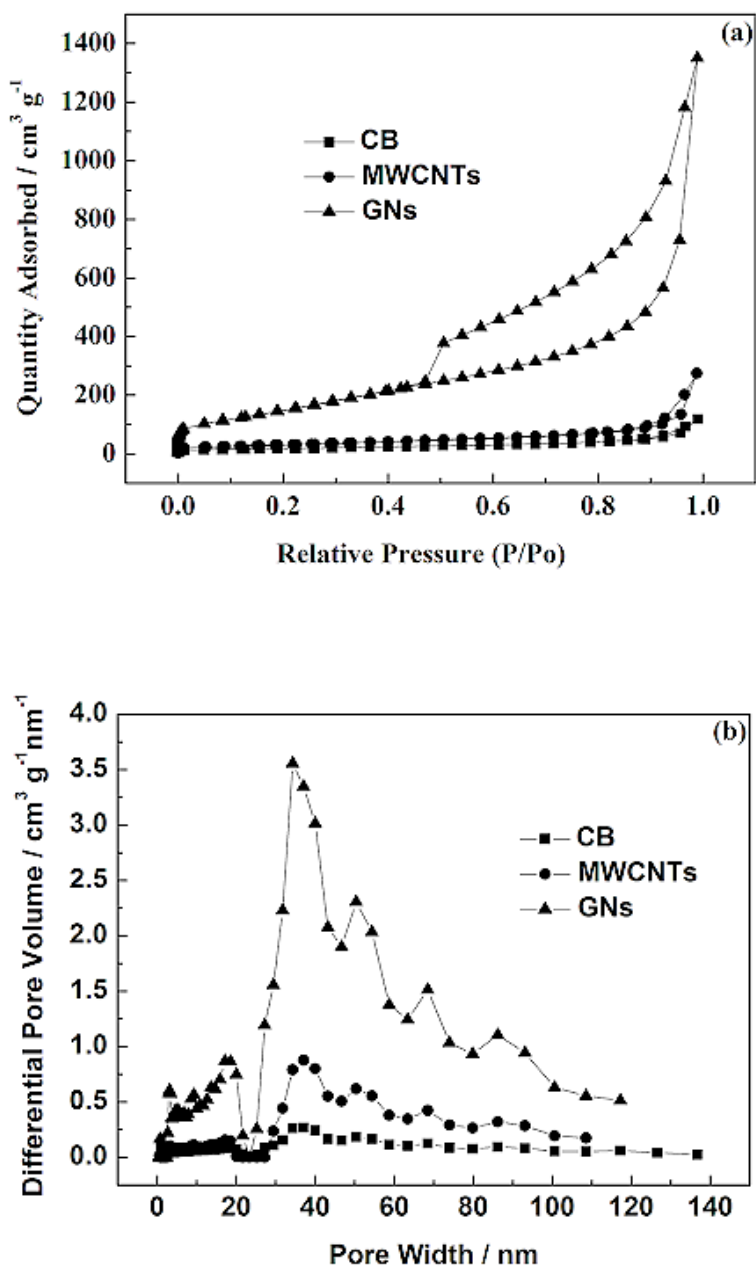


**Figure 2.** (a) Nitrogen adsorption/desorption isotherms of the three kind of carbonaceous conductive additives; (b) The pore size distribution of the three kind of carbonaceous conductive additives analyzed by Original Density Functional Theory Model.

The N<sub>2</sub> adsorption–desorption isotherms of the three kind of carbonaceous conductive additives are presented in Fig. 2(a). Different hysteresis loops in the nitrogen adsorption–desorption isotherms can be observed. Especially, the hysteresis loop of GNs resembles type H3 classification, resulting from slit-shaped pores between parallel layers [13]. The BET specific surface area, the total pore volume, and the average pore diameter of CB, MWCNTs and GNs are shown in Table 1.

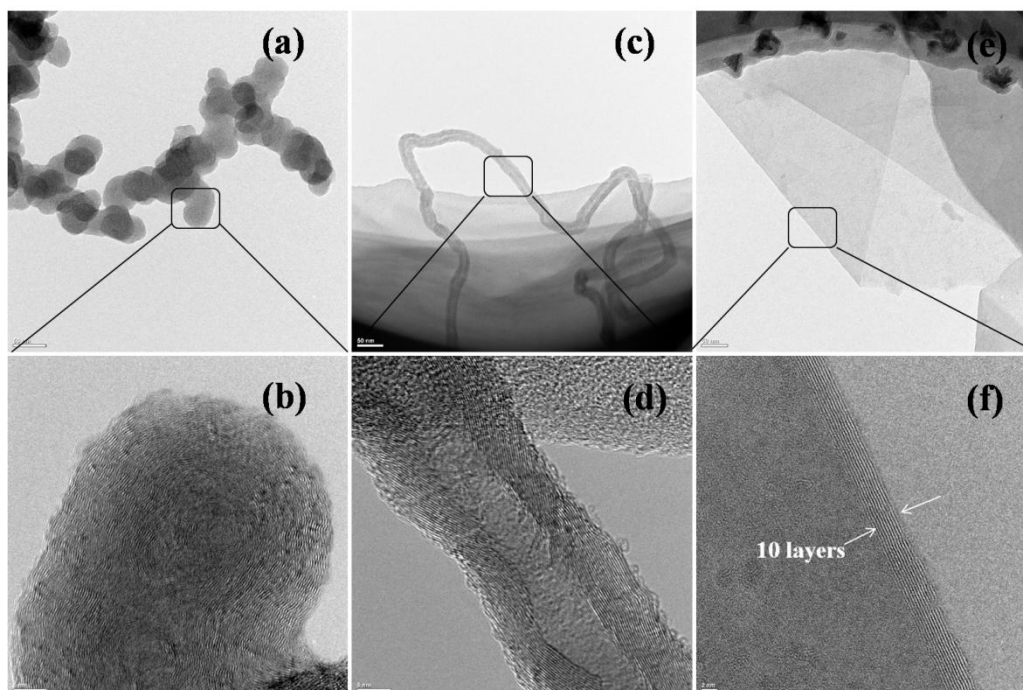


**Figure 3.** HRTEM images of (a, b) CB, (c, d) MWCNTs and (e, f) GNs.

The specific surface area of GNs is 575.3 m<sup>2</sup> g<sup>-1</sup>. The pore size distribution of the three kind of carbonaceous conductive additives analyzed by Original Density Functional Theory Model is exhibited in Fig. 2(b). From 0 to 20 nm, there is almost no difference between the curve of CB and CNTs. But in the case of GNs, the mesopores less than 20 nm in diameter, generated by rapid thermal exfoliation, make a big contribution to the increased pore volume. When the pore size is beyond 20 nm, the pore volume increased evidently and the total pore volume for GNs, CNTs, and CB is 2.08 cm<sup>3</sup> g<sup>-1</sup>, 0.42 cm<sup>3</sup> g<sup>-1</sup>, 0.18 cm<sup>3</sup> g<sup>-1</sup>, respectively.

The microstructures of CB, MWCNTs and GNs are characterized by HRTEM. In Fig. 3(a), CB aggregates together and stacks with each other to form long chains. As shown in Fig. 3(b), the fingerprint-like CB exhibits an amorphous carbon structure. Fig. 3(c) reveals that the external diameter of MWCNTs is 30~35 nm and the length is several micrometers in average. The HRTEM image of MWCNTs in Fig. 3(d) indicates that the MWCNTs are herringbone with turbulent layered structure. The HRTEM image of GNs in Fig. 3(e) indicates that GNs are folded and entangled with each other. Fig. 3(f) is the enlargement of the rectangle in Fig. 3(e). Some micropores and defects can be detected within the graphene nanosheets. The regular graphene domain demonstrates that GNs tend to stack in

the form of 10-12 layers, resulting in the thickness of around 3.5 nm. Heersche et al. reported that the electrons transport in GNs in the form of ballistic style, which is similar to the MWCNTs [14].

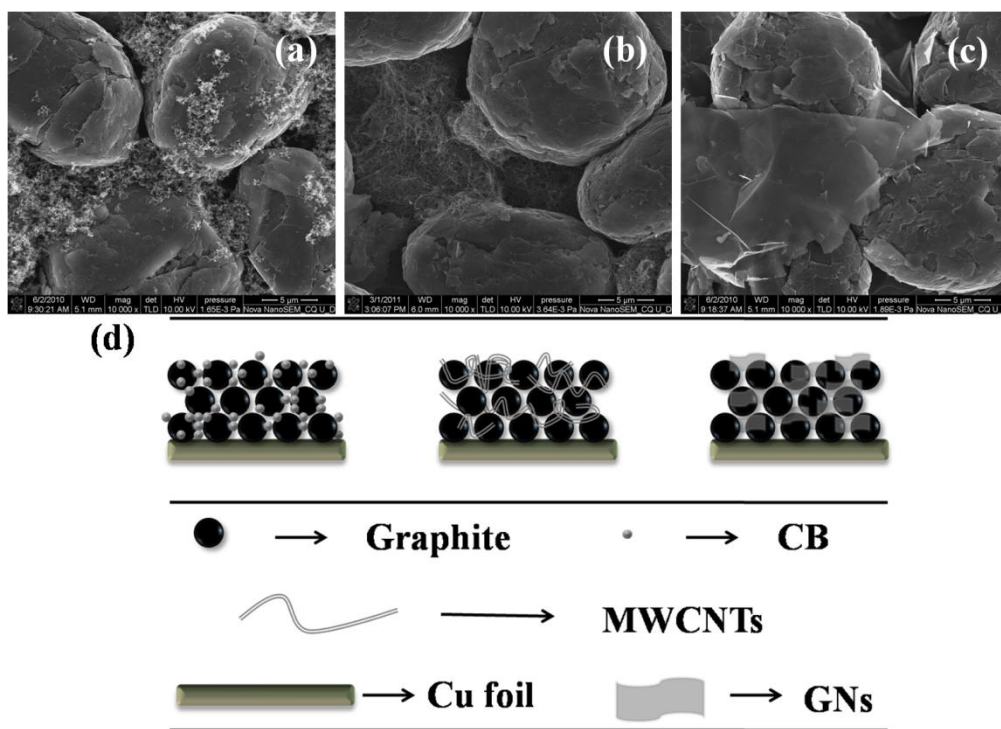


**Figure 4.** SEM images of electrode surfaces of (a) G-CB, (b) G-MWCNTs and (c) G-GNs; (d) the sketch of conductive network.

The morphologies of (a) G-CB, (b) G-MWCNTs and (c) G-GNs electrodes are exhibited in Fig. 4. In Fig. 4(a), CB agglomerates in the interval space among graphite particles and surrounds the spherical natural graphite. Some gaps also can be observed between the neighboring graphite particles, indicating potential interrupt of conducting routes. MWCNTs connect graphite particles together to form a three-dimensional network as shown in Fig. 4(b). It is clear that the network of MWCNTs appear in the interstitial grain-boundary region, which can improve the electrical continuity between graphite particles. In Fig. 4(c), the laminar GNs act as conducting bridges to cover the adjacent graphite particles in sheet.

Fig. 4(d) illustrates that the three kind of the network structure models of graphite mixed with different conductors. In the case of CB, zero-dimensional particles connect graphite particles following a “point-to-point” contact mode, where high loading and intimately contacted particles are needed to form effective electron conveying network. And the one-dimensional MWCNTs connect graphite particles together by a “line-to-line” mode, forming an effective conducting network. With respect to GNs, the two-dimensional ultrathin GNs can bridge active graphite particles by a “sheet-to-sheet” mode. Among the three kind of conducting modes, It is easy for GNs to form a conducting network with a low percolation threshold [15, 16].

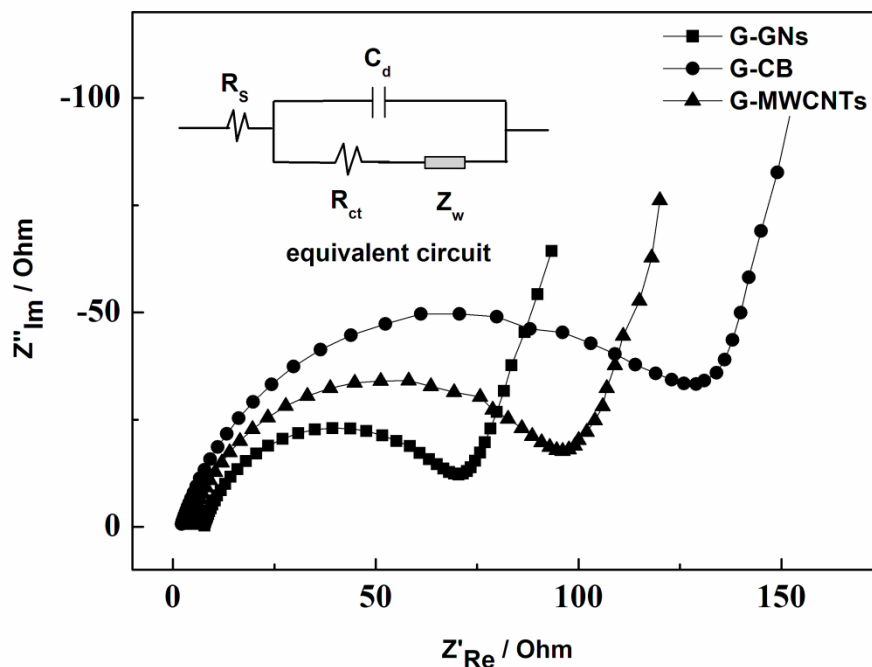


**Figure 5.** AC impedance spectra of G-CB, G-MWCNTs and G-GNs electrodes in three-electrode configuration in 1 M LiPF<sub>6</sub>/EMC-DEC (1:1 in vv<sup>-1</sup>) at 20 °C in the frequency range from 1 Hz to 100 kHz.

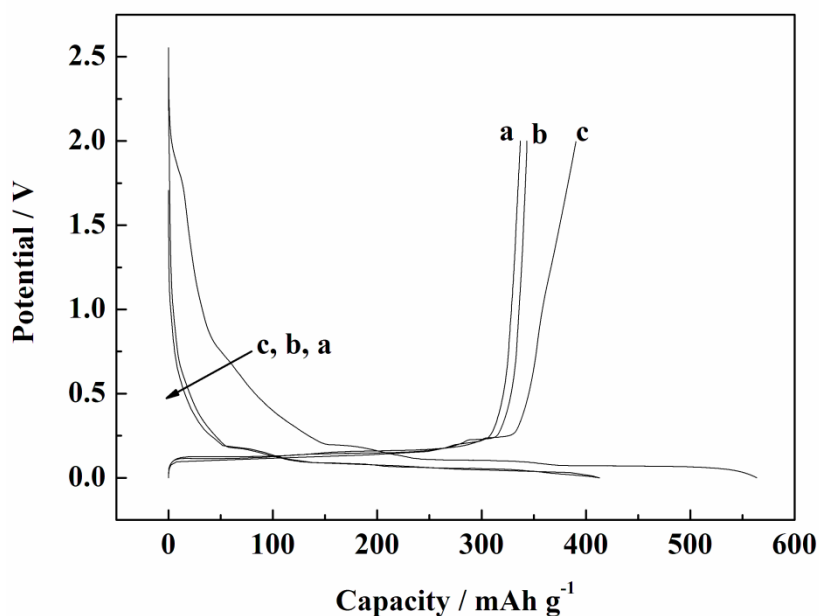


**Figure 6.** The first charge-discharge curves of (a) G-CB, (b) G-MWCNTs and (c) G-GNs electrodes in 1 M LiPF<sub>6</sub>/ EMC-DEC (1:1 in vv<sup>-1</sup>) at the cutoff voltage of 0.0-2.0 V vs. Li/Li<sup>+</sup> at 0.1 C rate.

As illustrated in Fig.5, the EIS spectra are combinations of a semicircle in high frequencies and a straight line in low frequencies with the equivalent circuit on the left. The symbols  $R_s$ ,  $R_{ct}$ ,  $C_d$ , and  $Z_w$ , represent the solution resistance, charge-transfer resistance, capacitance of the double layer, and

Warburg impedance, respectively. In the medium frequency region, the intercepts with real impedance  $[\text{Re}(Z)]$  axis of G-CB, G-MWCNTs, and G-GNs is 129 Ohm, 95 Ohm, and 71 Ohm, respectively, which is believed to be the total electronic resistance of the electrode materials [9, 17]. The decrease of the semicircles can be attributed to the facile formation of conductive network by MWCNTs or GNs. Furthermore, GNs possess higher electron transfer kinetics than MWCNTs due to high aspect ratio and  $\text{sp}^2$  carbon lattice.

Fig.6 shows the first charge-discharge curves of (a) G-CB, (b) G-MWCNTs and (c) G-GNs electrodes at 0.1 C rate. The 1<sup>st</sup> charge capacity was  $337 \text{ mAh g}^{-1}$ ,  $343 \text{ mAh g}^{-1}$ ,  $366 \text{ mAh g}^{-1}$  and the initial cycle efficiency was 91%, 83%, and 67% for G-CB, G-MWCNTs and G-GNs electrodes, respectively. The charge capacity of G-GNs is the biggest, which could attributed to the enlarged interlayer spacing of GNs, widening the  $\text{Li}^+$  diffusion route. When the graphene layer distance is increased, it might provide a bigger  $\text{Li}^+$  accommodation amount than that of the limited  $\text{LiC}_6$  stage 1 compounds [18]. The reversible capacity is effectively increased in the case of G-MWCNTs and G-GNs electrodes, but the initial cycle efficiency need to be improved. The initial irreversible capacity loss occurs at 0.8 V vs.  $\text{Li/Li}^+$  in discharge curves. It is commonly believed that the solvent reduction products, such as  $\text{Li}_2\text{CO}_3$  or  $(\text{CH}_2\text{OCO}_2\text{Li})_2$ , precipitate on the carbon surface to form a solid electrolyte interface (SEI), leading to the irreversible capacity loss [19-22]. The decrease of irreversible capacity loss can be ascribed to the reduction of the specific surface areas (as shown in Table 1) [23].

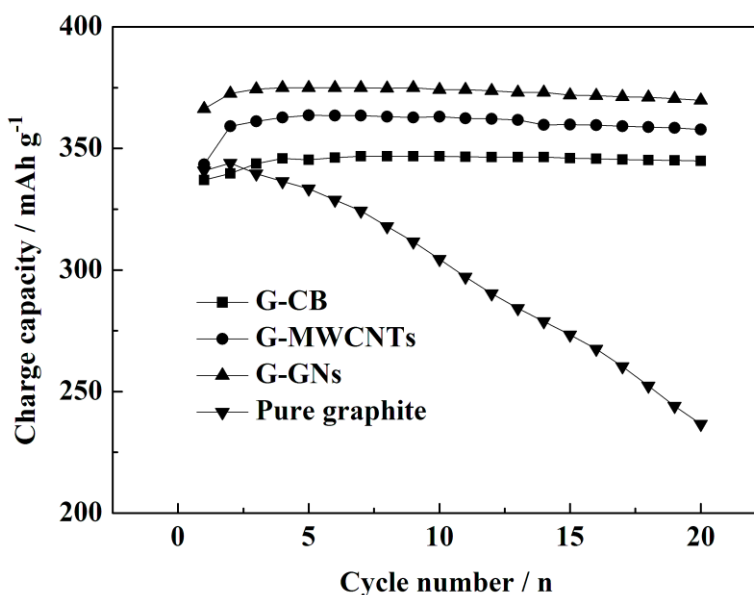


**Figure 7.** Cycling performance of pure graphite, G-CB, G-MWCNTs and G-GNs electrodes in 1 M  $\text{LiPF}_6$  / EMC-DEC (1:1 in  $\text{v v}^{-1}$ ) at the cutoff voltage 0.0-2.0 V vs.  $\text{Li/Li}^+$ .

Fig.7 shows the cycling performance of the graphite anode mixed with different conductors. We find that the bare graphite shows poor electrochemical properties for lithium ion batteries. The

specific capacity of the bare graphite drops slightly from 343 mAh g<sup>-1</sup> in the 2<sup>nd</sup> cycle to 236 mAh g<sup>-1</sup> in the 20<sup>th</sup> cycle.

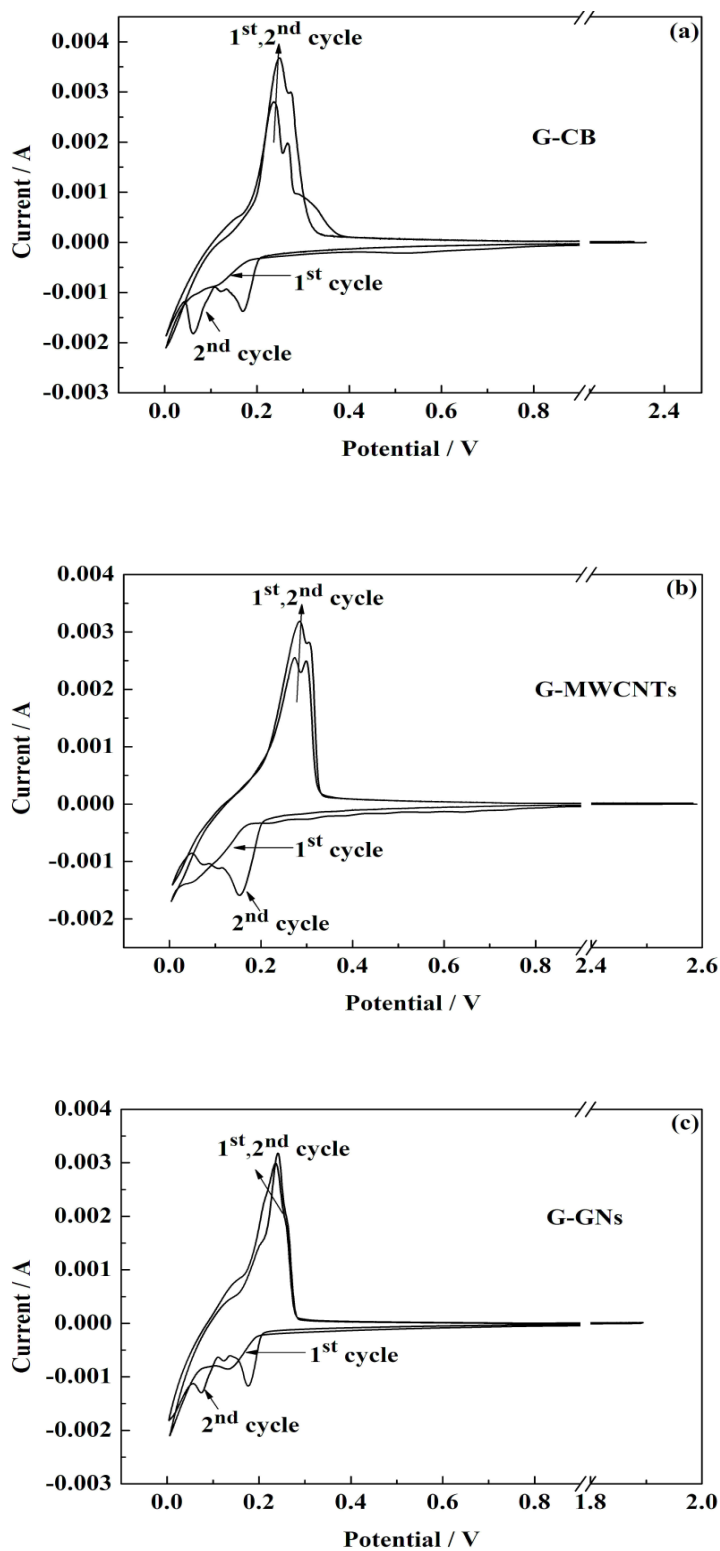


**Figure 8.** Cyclic voltammetry for the first 2 cycles obtained from (a) G-CB, (b) G-MWCNTs and (c) G-GNs electrodes in 1 M LiPF<sub>6</sub> / EMC-DEC (1:1 in vv<sup>-1</sup>) at 0.05 mVs<sup>-1</sup> scanning rate in 0.0-2.0 V vs. Li/Li<sup>+</sup> sweep range.

In the process of solvent  $\text{Li}^+$  insertion-deinsertion, graphite particles repeatedly expand-contract and the volume changes severely, leading to the decline of the cycle stability [24]. When carbon conductors are added in graphite, both the reversible capacity and cycle stability are improved remarkably. After 20 cycles, the reversible capacity of G-GNs, G-MWCNTs and G-CB still maintains at  $369 \text{ mAh g}^{-1}$ ,  $357 \text{ mAh g}^{-1}$ , and  $344 \text{ mAh g}^{-1}$ , respectively. The network composite of spherical graphite with carbon conductors is effective to improve the electrochemical activity of  $\text{Li}^+$  intercalation/de-intercalation, especially in the GNs mode. Multilayer GNs tend to overlap and wrinkle, leading to the nanochannels and micropores, which are expected to provide paths for  $\text{Li}^+$  insertion and extraction.

In Fig. 8, all the three cyclic voltammetry curves unfold a typical CV of graphitic structure. The clearly sliding curve in the 1<sup>st</sup> cycle at the potential range of 0-0.8 V could be ascribed to the  $\text{Li}^+$  consumption on the formation of solid electrolyte interface (SEI) [19-22, 25]. The lithium insertion into graphite occurs below 0.3 V versus  $\text{Li}/\text{Li}^+$ . There are three cathodic peaks in the 2<sup>nd</sup> cycle: 0.18 V, 0.12 V, 0.06 V, accordingly, generating the intercalation compounds:  $\text{LiC}_{27}$ ,  $\text{LiC}_{12}$ , and  $\text{LiC}_6$  [24, 26]. In Fig. 8(a), there are two anodic peaks at 0.22 V and 0.25 V for G-CB. With the increase of the cycles, the intensity of the anodic peak at 0.22 V significantly increases, at the same time, the anodic peak at 0.25 V gradually disappears. In Fig. 8(b), the weakly cathodic peak of G-MWCNTs at 0.06 V is little different from G-CB and G-GNs, which probably engenders by the different conductive mode. As shown in Fig. 8(c), there is only one anodic peak at 0.22 V for G-GNs.

#### 4. CONCLUSIONS

Three kind of carbonaceous conductive additives in different dimension, such as CB, MWCNTs and GNs, were added in spherical graphite to form different network nanocomposite. The comparative investigation demonstrated that the addition of conducting additives improved both reversible capacity and cycling stability remarkably. Among the three kind of carbonaceous conductive additives, GNs bridge graphite particles by a “sheet-to-sheet” mode, which were the most effective to decrease the resistance and to improve electrochemical behaviors.

The research is of potential interest to application of GNs as a new conducting additive in electrode preparation and to development of high-power lithium ion batteries for electric vehicles.

#### ACKNOWLEDGEMENTS

We are grateful for the financial support from Project No.CDJZR10 13 88 01 & No.CDJXS10 13 11 58 of the Fundamental Research Funds for the Central Universities and for the Natural Science Foundation of China (No.51172293).

#### References

1. M. Armand and J.M. Tarascon, *Nature*, 451 (2008) 652.
2. J. Maier, *Nat. Mater.*, 4 (2005) 805.

3. R. Dominko, M. Gaberscek, J. Drofenik, M. Bele and J. Jamnik, *Electrochim. Acta*, 48 (2003) 3709.
4. A. Momchilov, A. Trifonova, B. Banov, B. Pourecheva and A. Kozawa, *J. Power Sources*, 81 (1999) 566.
5. A.G. Pandolfo, G.J. Wilson, T.D. Huynh and A.F. Hollenkamp, *Fuel Cells*, 10 (2010) 856.
6. C.A. Frysz, X.P. Shui and D.D.L. Chung, *J. Power Sources*, 58 (1996) 41.
7. D.H. Jang and S.M. Oh, *Electrochim. Acta*, 43 (1998) 1023.
8. B. Jin, E.M. Jin, K.H. Park and H.B. Gu, *Electrochem. Commun.*, 10 (2008) 1537.
9. X.L. Li, F.Y. Kang, X.D. Bai and W. Shen, *Electrochem. Commun.*, 9 (2007) 663.
10. F.Y. Su, C.H. You, Y.B. He, W. Lv, W. Cui, F.M. Jin, B.H. Li, Q.H. Yang and F.Y. Kang, *J. Mater. Chem.*, 20 (2010) 9644.
11. W.S. Hummers and R.E. Offeman, *J. Am. Chem. Soc.*, 80 (1958) 1339.
12. K. Sato, M. Noguchi, A. Demachi, N. Oki and M. Endo, *Science*, 264 (1994) 556.
13. S.M. Paek, E. Yoo and I. Honma, *Nano Lett.*, 9 (2009) 72.
14. H.B. Heersche, P. Jarillo-Herrero, J.B. Oostinga, L.M.K. Vandersypen and A.F. Morpurgo, *Nature*, 446 (2007) 56.
15. E.J. Garboczi, K.A. Snyder, J.F. Douglas and M.F. Thorpe, *Physical Review E*, 52 (1995) 819.
16. S. Stankovich, D.A. Dikin, G.H.B. Dommett, K.M. Kohlhaas, E.J. Zimney, E.A. Stach, R.D. Piner, S.T. Nguyen and R.S. Ruoff, *Nature*, 442 (2006) 282.
17. C.Y. Lee, H.M. Tsai, H.J. Chuang, S.Y. Li, P. Lin and T.Y. Tseng, *J. Electrochem. Soc.*, 152 (2005) A716.
18. E. Yoo, J. Kim, E. Hosono, H. Zhou, T. Kudo and I. Honma, *Nano Lett.*, 8 (2008) 2277.
19. D. Aurbach, H. Teller and E. Levi, *J. Electrochem. Soc.*, 149 (2002) A1255.
20. D. Aurbach, A. Zaban, Y. Ein-Eli, I. Weissman, O. Chusid, B. Markovsky, M. Levi, E. Levi, A. Schechter and E. Granot, *J. Power Sources*, 68 (1997) 91.
21. S.H. Ng, C. Vix-Guterl, P. Bernardo, N. Tran, J. Ufheil, H. Buqa, J. Dentzer, R. Gadiou, M.E. Spahr, D. Goers and P. Novak, *Carbon*, 47 (2009) 705.
22. W.B. Xing and J.R. Dahn, *J. Electrochem. Soc.*, 144 (1997) 1195.
23. Y.S. Park, H.J. Bang, S.M. Oh, Y.K. Sun and S.M. Lee, *J. Power Sources*, 190 (2009) 553.
24. D. Aurbach, B. Markovsky, I. Weissman, E. Levi and Y. Ein-Eli, *Electrochim. Acta*, 45 (1999) 67.
25. F.M. Wang, M.H. Yu, Y.J. Hsiao, Y. Tsai, B.J. Hwang, Y.Y. Wang and C.C. Wan, *Int. J. Electrochem. Sci.*, 6 (2011) 1014.
26. M.D. Levi and D. Aurbach, *J. Phys. Chem. B*, 101 (1997) 4630